BL-27A/2016G188, 2018G085

Depth Concentration Profile for Cesium Atom in Fullerene C_{60} Investigated Using Synchrotron X-ray Photoelectron Spectroscopy

Tetsuhiro SEKIGUCHI[1,*], Keiichi YOKOYAMA[1] and Tsuyoshi YAITA[1]
[1] Materials Science Research Center, Japan Atomic Energy Agency, 2-4 Shirakata, Tokai-mura, Naka-gun, Ibaraki, 319-1195, Japan

1 Introduction

The Cesium-135 (^{135}Cs) with a half-life of 2.3 million years is contained in nuclear wastes, thus is an important target for nuclear transmutation [1]. In prior to it, isotope separation of ^{135}Cs from stable ^{133}Cs is indispensable. Thus, technology development of the isotopic separation is important not only for nuclear transmutation, but also for volume reduction of wastes to be disposed geologically.

In the course of separation processes in the gas phase isotope selective photo-dissociation [2], it is needed to avoid collision induced isotope-exchange [3] between active ^{135}Cs atom and stable ^{133}CsI. Thus, to avoid collision, we tried to selectively absorb Cs atom into deep carbon materials.

We have investigated depth concentration distributions of Cs atom in absorbent fullerene solids (C_{60}) using angle-resolved (AR) [4], X-ray energy dependent (ED), or Sputter-time dependent X-ray photoelectron Spectroscopy (XPS). Presently we report on the results of AR-XPS experiments.

2 Experiment

Experiments were performed at BL27A of Photon Factory. An analyzing chamber (base pressure 1×10^{-7} Pa) was equipped with XPS system with a spherical electron energy analyzer (VSW Co., CLASS100) and a sputter ion-gun. The preparation chamber was equipped with K-cells (AVC Co.) for C_{60} (Aldrich Co., 99%) and CsI (Kanto Chem. Co., 99.99%), and Cs alkali metal dispenser (SAES Co., CS/NF/3.9/12FT10), a thickness monitor (INFICON Co., STM/2), and a quadrupole mass spectrometer (SRS Co., RGA200) for monitoring relative flux of Cs or CsI species during deposition. Sample films were prepared in the vacuum chamber, and transferred to the analyzing chamber that was connected to synchrotron beam-line.

Si(111) substrates were cleaned by repeated Ar_+-sputtering. Through the K-cell heated at 750 K, C_{60} was grown on the Si substrates. On C_{60} films, Cs atom or CsI was dosed from the SAES getter source (Cs_2CrO_4) or CsI powder, respectively. Typical deposition rates were ca. 0.02 Å/sec (C_{60}), 0.03 Å/sec (Cs), and 0.005 Å/sec (CsI), which were recorded by the thickness monitor.

3 Results and Discussion

Figures 1a and 1b show X-ray photoelectron spectra for a Cs dosed C_{60} (hereafter, we abbreviate it as Cs/C_{60}) film and for CsI deposited on C_{60} (CsI/C_{60}), respectively, which cover Cs $3d_{5/2,\ 3/2}$, I $3d_{5/2,\ 3/2}$, and C 1*s* regions. To obtain depth concentration profiles of Cs atom, photoelectron spectra were measured at various electron emission angles (θ), defined as angles between the electron energy analyzer direction and the surface normal. It has been found that relative intensity of C 1s to Cs 3d depends on θ for CsI/C_{60}, while it scarcely depends for Cs/C_{60}. In Fig. 1b, relative intensity of C 1*s* peak is one order of magnitude smaller at θ = 68° than at θ = 7°.

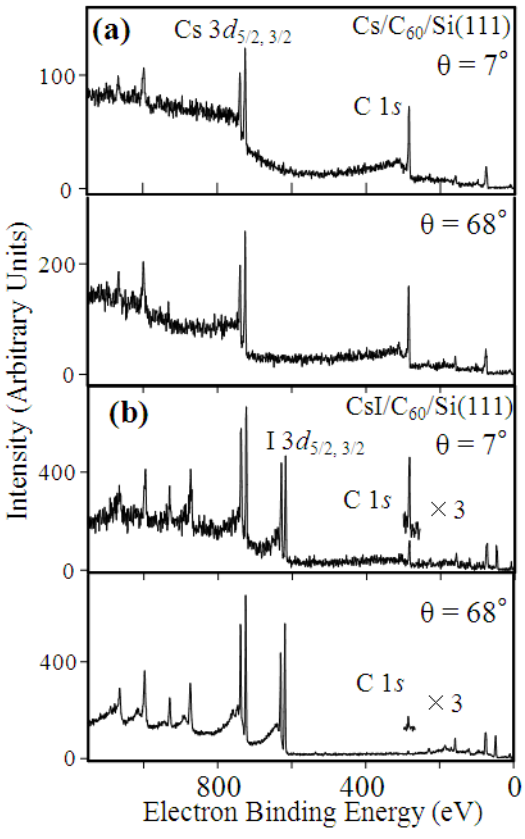

Figure 1 X-ray photoelectron spectra measured with photon energy of 2200 eV for (**a**) Cs-dosed on C_{60} film and for (**b**) CsI-deposited on C_{60} film. Electron emission angles (θ) are indicated on the right top.

This difference is further evidenced in Figure 2 that shows integrated intensities of Cs $3d_{5/2,3/2}$ (or I $3d_{5/2,3/2}$) and C 1*s* (labelled ×) plotted as a function of

θ, although there was a trend that detection efficiencies decrease with increasing θ. In Fig. 2, plotted were photoelectron intensities corrected by analyzer transmission functions (F) and by theoretical partial photoionization cross sections (σ) for hν = 2200 eV photon [5]. Hereafter, we indicate these corrected values simply as intensities.

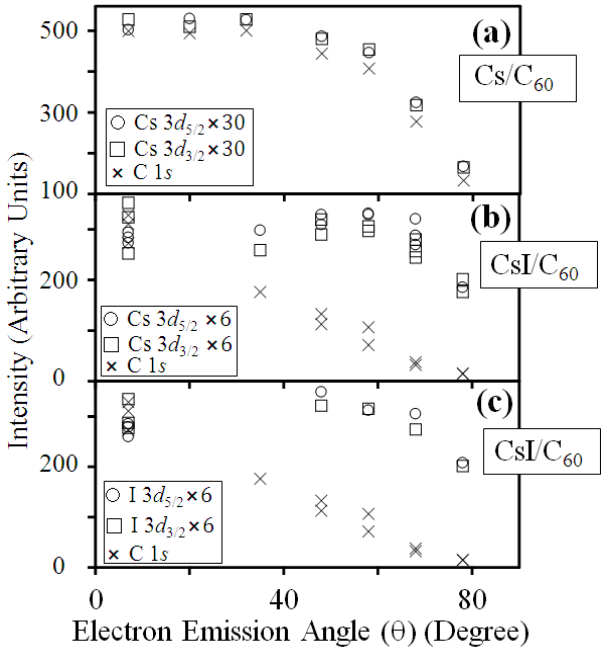

Figure 2 (**a**) Intensities of Cs 3*d*5/2, 3/2 and C 1*s* peaks as a function of electron emission angles θ, which were measured for Cs–dosed C_{60} film. Intensities of (**b**) Cs 3*d*5/2, 3/2 and C 1*s* and (**c**) I 3*d*5/2, 3/2 and C 1*s* peaks measured for CsI- deposited C_{60} film.

As for Cs/C_{60} (Fig. 2a), a key finding is the fact that the angular dependence of C 1*s* relative intensities (labelled ×) is not prominent. In addition, the angular dependence of C 1*s* is similar to that of Cs 3*d*5/2,3/2 intensities, suggesting that concentrations of cesium and carbon do not significantly change in shallow and deep regions.

In contrast, as for CsI/C_{60} (Fig. 2b and 2c), the relative intensities of C 1*s* peak (labelled ×) gradually decrease with increasing θ. This observation can be qualitatively explained by the fact that detection depths become shallow at large θ. Observation depths is about 171 Å for θ = 7°, while that decreases to 33 Å for θ = 78°. Thus, it is suggested that the concentration of carbon is lower at shallow surface region compared at deep.

The purpose of angle dependence measurement is to obtain depth profile, f(z), which is defined as the atomic density at depth z. The integrated photoelectron intensity I(θ) at various angles θ can be expressed in the following equation [6]:

$$I(\theta) = \frac{F \cdot D \cdot A \cdot K(\theta)}{\cos\theta}\sigma\int_0^{\infty} dz\ f(z)\ \exp\left(\frac{-z}{\lambda(z)\cos\theta}\right) \quad (1)$$

where D is the detection efficiency, K includes X-ray flux and other dependencies related with the instrument. Parameters F, D, and K can be eliminated by expressing intensities as fractional intensities, e.g. $I_{Cs3d}/(I_{Cs3d} + I_{C1s})$.

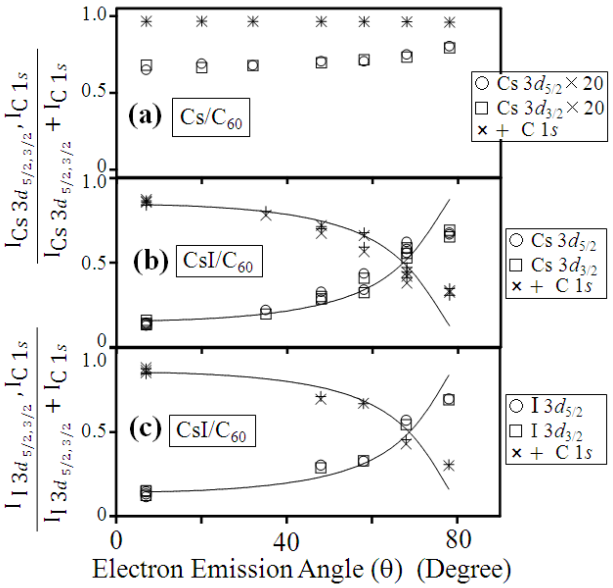

Figure 3 Fractional intensities, e.g. $I_{Cs3d}/(I_{Cs3d} + I_{C1s})$, of (**a**) Cs 3*d*5/2, 3/2 peaks as a function of electron emission angles (θ), which were measured for Cs- dosed C_{60} film. Those of (**b**) Cs 3*d*5/2, 3/2 and (**c**) I 3*d*5/2, 3/2 peaks measured for CsI-deposited C_{60} film. Full lines show the best fitted curves calculated by assuming a uniform CsI-over-layered model.

Figure 3 shows fractional intensities of Cs 3*d*5/2, 3/2, I-3*d*5/2, 3/2, and C 1*s* for Cs/C_{60} (Fig. 3a) and CsI/C_{60} (Fig.-3b, 3c). We can now clearly see that angular dependence in Cs 3*d*5/2, 3/2, or C 1*s* is very scarce for Cs/C_{60}, while angle dependence in Cs 3*d*5/2, 3/2 (or I 3*d*5/2, 3/2), or C 1*s* is marked for CsI/C_{60}. Moreover, the results provide evidence for the fact that C 1*s* relative intensity for CsI/C_{60} decreases with increasing θ. These observations consistently support the view that Cs was mixed into C_{60} bulk in Cs/C_{60}, whilst CsI was deposited on C_{60} surface forming over-layer in CsI/C_{60}.

As for CsI/C_{60} we confirm whether over-layered model is suitable or not in more quantitative manner. In this model, a uniform CsI film is formed on the C_{60} surface. The intensity of Cs 3*d* or C 1*s* is expressed as,

$$I(Cs3d) = K(\theta)\sigma(Cs3d)\lambda_{CsI}(Cs3d)\, n(Cs)\left[1-\exp\left(\frac{-d}{\lambda_{CsI}(Cs3d)\cos\theta}\right)\right] \quad (2)$$

$$I(C\,1s) = K(\theta)\sigma(C\,1s)\lambda_{C60}(C\,1s)\, n(C)\exp\left(\frac{-d}{\lambda_{CsI}(C\,1s)\,\cos\theta}\right) \quad (3)$$

where *d* is thickness of postulated CsI over-layer, K(θ) includes angular dependent coefficient related with the instrument. K(θ) can be vanished by expressing intensities as fractional intensities. We fit the equations (2) and (3) to experimental measurements and evaliate *d* as parameters. IMFP values aere calculated as follows: λ_{CsI}(Cs 3$d_{5/2,3/2}$) = 46.4 Å, λ_{CsI}(I 3$d_{5/2,3/2}$) = 49.1 Å, λ_{CsI}(C 1*s*) = 57.2 Å, λ_{C60}(C 1s) = 45.2 Å for hν = 2200 eV based on TPP2M method [7]. Atomic densities are n(Cs) = 1.73×10^{-2} and n(C) =0.143 [mol cm^{-3}] for crystalline CsI and C_{60}, respectively. Figures 3b and 3c depict the best-fit curves which give the thickness (*d*) of CsI over-layer being 48 Å (Cs 3$d_{5/2}$), 46 Å (Cs 3$d_{3/2}$), 44Å (I 3$d_{5/2}$), and 43 Å (I 3$d_{3/2}$) for CsI/C_{60}. It is noteworthy that Cs 3$d_{5/2,\ 3/2}$ and I 3$d_{5/2,\ 3/2}$ data gave consistent thickness. As for Cs/C_{60} (Fig 3a), on the other hand, the fitting routine could not find any suitable solutions or ended in barely convergent with large parameter errors. This suggests that over-layer hypothesis is not valid for Cs/C_{60}.

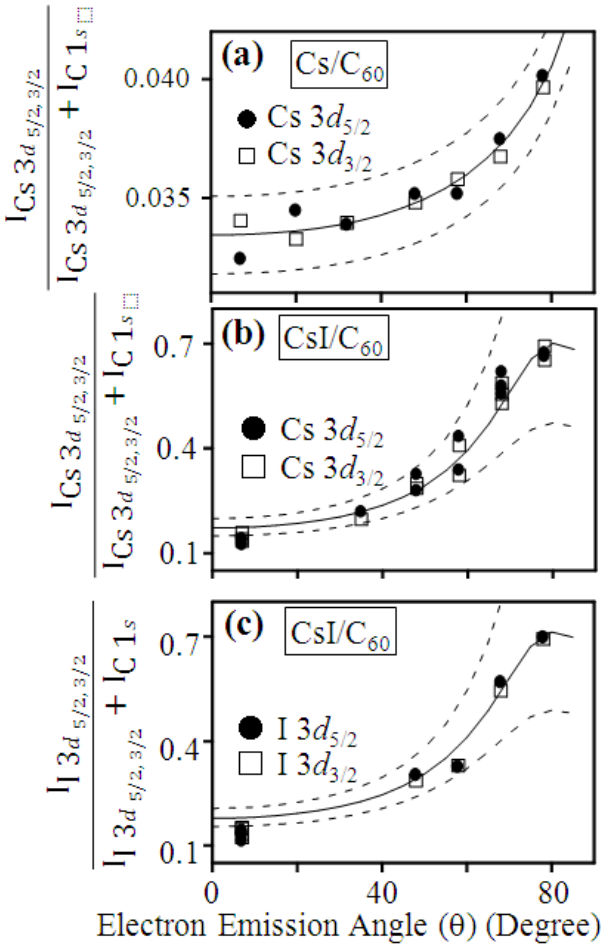

Fig. 4: Enlarged fractional intensity plots of (a) Cs 3$d_{5/2,3/2}$ peaks for Cs–dosed C_{60} film, along with the best fit curves. Those of (b) Cs 3$d_{5/2,\ 3/2}$ and (**c**) I 3$d_{5/2,\ 3/2}$ for CsI-deposited C_{60} film. Broken lines show curves assuming ±6% deviations from the best Cs molar fractions.

To understand how Cs atoms mix with C_{60} molecules, we tried to convert the angle-dependent photoemission intensities to Cs concentrations as a function of depth. We postulated a model depth profile containing concentration gradients constructed from linear segments, which has been originally modelled by Paynter [6]. This model contains the quantities of concentrations c_i at the depth z_i; i = 1, 2, or 3 for the three segment model was taken into account in our analysis. The quantities of concentrations c_i were expressed as molar fraction, which is defined as follows:

$$C_i(Cs) = \frac{[Cs]_i}{[Cs]_i + [C_{60}]_i} \quad , \quad C_i(CsI) = \frac{[CsI]_i}{[CsI]_i + [C_{60}]_i} \quad (4)$$

The intensity calculation takes the sum over each linear segment; that is,

$$I = I_1(c_1,\ z_1(=0) \rightarrow c_2, z_2) + I_2(c_2, z_2 \rightarrow c_3, z_3) + I_3(c_3,\ z_3 \rightarrow c_3,\ \infty) \quad (5)$$

We profiled cesium distributions by the procedure described below. First, integration in Eq. (1) was numerically calculated as a function of θ. Thus, angular profiles of fractional intensities, that is $I_{Cs3d}(\theta)/[I_{Cs3d}(\theta)+ I_{C1s}(\theta)]$, were obtained. Next, the sums of weighted squares error (chi squares) were calculated,

$$\chi^2 = \sum_k \frac{(Fr_k^{calc} - Fr_k^{obs})^2}{\sigma_k^2} \quad (6)$$

where σ_k represents the standard deviation in the k-th measurement at an angle θ_κ; and Fr_k^{calc} and Fr_k^{obs} show calculated and experimental fractional intensities, respectively. The aforementioned calculations were repeated until the chi squares were minimized using a least squares fitting routine by Levenberg-Marquardt algorithm. For Cs/C_{60} and CsI/C_{60} both, inelastic mean free paths, IMFPs that is, $\lambda_{mixture}$(Cs 3*d*) and $\lambda_{mixture}$(C 1*s*), were calculated based on TPP2M formulae, in which dependencies of λ on Cs concentration or depth z were taken into account. This treatment improves accuracy of 10 or 20%. In calculating λ for $(Cs)_nC_{60}$, density was corrected by approximated linear relation between its molecular weight and density under n< 8 [8], where a symbol 'n' indicates an index for $(Cs)_nC_{60}$.

Figures 4a - 4c show the best fitted fractional intensity curves. Figures 5a - 5e show the optimized solution of depth profiles in the unit of molar fraction for Cs or CsI versus C_{60}.

It is known that depth profile is not uniquely determined from a set of experimental data [6]. Even so, characteristics were roughly reproduced to be different between Cs/C_{60} and CsI/C_{60}. As for Cs/C_{60}, concentration $c_3(Cs) = 0.68$ (molecular fraction) at $z_3 = 32$ Å ⟶ ∞ tends to be close to $c_2(Cs) = 0.73$ at $z_2 = 8$ Å, suggesting that the Cs concentration is maintained to bulk as shown in Fig. 5a. As typical value, $Cs_{3.6}C_{60}$ at surface and $Cs_{2.2}C_{60}$ at bulk were estimated for Cs/C_{60} as shown in Fig. 5c. In contrast, as for CsI/C_{60} the concentration $c_3(CsI) = 0.0$ at $z_3 = 47$ Å tends to be nearly zero, as shown in Fig. 5d. Although a certain amount of CsI was deposited on the C_{60} surface, we consider that CsI molecule does not penetrate into bulk, but stops at a barrier interface between CsI and C_{60} phases.

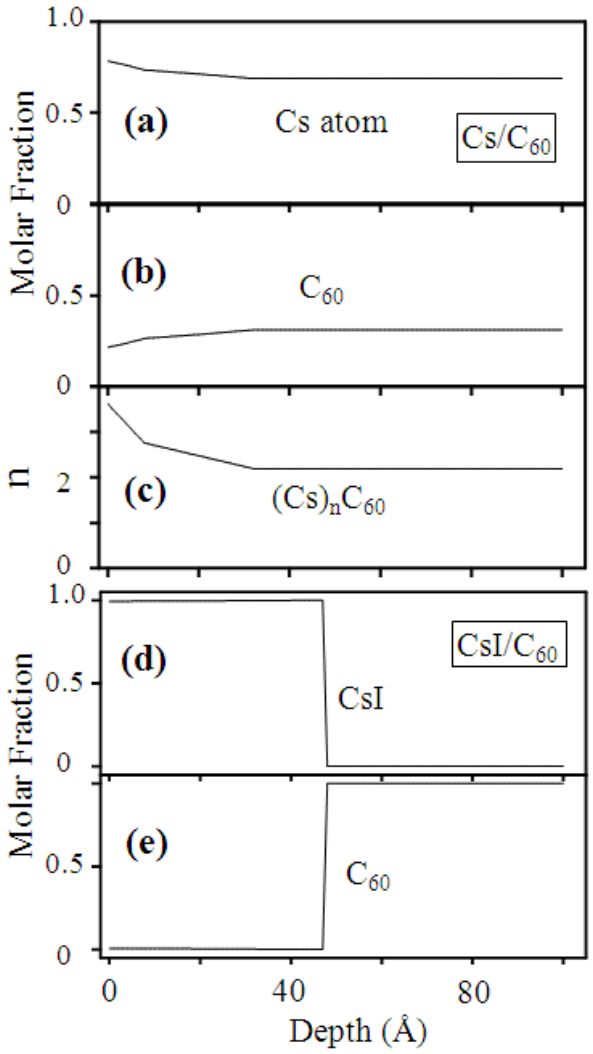

Fig. 5: The most probable depth molar-fractional profiles (a), (b), and ratio n (c) for Cs–dosed C_{60} film and those (d) and (e) for CsI-deposited C_{60} film.

In conclusion, we investigated the property of C_{60} solid as an absorbent for Cs atom or CsI molecule using the angle-resolved XPS technique. Angular independencies were observed for Cs-dosed C_{60}, while over-layer-like angular dependencies were recorded for CsI-deposited C_{60}. This observed difference was interpreted as the different penetrating abilities between Cs and CsI into the C_{60} solid. Thus, the present results show that C_{60} can become a candidate absorbent as Cs-selective material that prevents ^{135}Cs and ^{133}CsI from collision. For realizing the ideal situation that CsI does not stick on the C_{60} surface, heating experiments are in progress.

Acknowledgement

The authors wish to thank Drs. Y. Okamoto, M. Honda, I. Shimoyama of JAEA, Prof. N. Usami and the staff of Photon Factory KEK for the helpful support during synchrotron experiments performed

under PF-PAC (No. 2016G188 and 2018G085). This work was supported by JSPS KAKENHI [grant number 15H02345].

References

[1] S. Ohki and N. Takaki, *7-th Information Exchange Meeting on Actinide and Fission Product Partitioning and Transmutation*, *OECD/NEA* No. 5990, Oct. 2002, Jeju, Repub. Korea, (2002), pp.14-16.
[2] L. Matsuoka, A. Ichihara, M. Hashimoto, and K. Yokoyama, Proc. GLOBAL2011, Makuhari, Japan, Dec. 11-16 (2011), Paper No. 392063, pp. 1 - 7.
[3] T. Kobayashi, M. Hashimoto, and K. Yokoyama, *JAEA-Research*, 2015-014, (2015), pp. 1-7 (*in Japanese).*
[4] T. Sekiguchi *et al*., *Prog. Nucl. Sci. Tech.* **5**, 161 (2018).
[5] J.H. Scofield, *Lowrence Livermore Laboratory Report, TID-4500, UC-34 Physics*, UCRL-51326 (1973), pp. 144-147.
[6] R.W. Paynter, Modification of the Beer-Lambert equation for application to concentration gradients, *Surf. Interf. Anal*. 3 (1981), pp. 186-187.
[7] S. Tanuma, C.J. Powell, and D.R. Penn, *Surf. Interf. Anal*. 21 (1994), pp.165-176.
[8] H-N. Li, X-X. Wang, and W-F. Ding, *J. Elect. Spect. Relat. Phenom.* 153 (2006), pp. 96-101.

* sekiguchi.tetsuhiro@jaea.go.jp